Effect of ac Electrodeposition Conditions on the Growth of High Aspect Ratio Copper Nanowires in Porous Aluminum Oxide Templates

Nathan J. Gerein and Joel A. Haber*

Department of Chemistry, University of Alberta, Edmonton, Alberta, Canada, T6G 2G2

Received: March 14, 2005; In Final Form: July 16, 2005

The effect of several deposition parameters on the uniformity of copper electrodeposition through the alumina barrier layer into porous aluminum oxide templates grown in sulfuric or oxalic acid was systematically investigated. A fractional factorial design of experiment was conducted to find suitable deposition conditions among the variables: frequency, voltage, pulsed or continuous deposition, electrolyte concentration, and barrier layer thinning voltage. Continuous ac sine wave deposition conditions yielded excellent uniformity of pore-filling but damaged the porous aluminum oxide templates when deposition was continued to grow bulk copper on the surface. Pulsed electrodeposition yielded comparable uniformity of pore-filling and no damage to the porous aluminum oxide templates, even when bulk copper was deposited on them. Further optimization of pulsed deposition conditions was accomplished by comparing square and sine waveforms and pulse polarity. Pulsed square waveforms produced better pore-filling than pulsed sine waveforms. For sine wave depositions, the oxidative/reductive pulse polarity was more efficient than the commonly used reductive/oxidative pulse polarity. For square wave depositions into sulfuric acid grown pores, the reductive/oxidative pulse polarity produces more uniform pore-filling, likely as a result of enhanced resonant tunneling through the barrier layer and reoxidation of copper in faster filling pores.

Introduction

Template-directed syntheses utilizing porous aluminum oxide (PAO) templates have become a popular pathway to diverse nanostructured materials.[1−3] PAO templates are easily fabricated and offer the benefit of high pore densities in a hexagonal close-packed array and the ability to tailor pore diameters and depths.[4−6] Following the pore-filling process, the PAO host may be removed via dissolution in either acid or base, permitting the preservation of most guest materials. Deposition into the pores using direct current (dc) electrodeposition conditions has proven to be a particularly powerful technique, enabling substantial control over composition and crystallinity,[7] and easy access to compositional modulation along the wire lengths.[8] However, none of the dc techniques reported to date are amenable to industrial scale processing because of the laborious preprocessing that must be performed on the PAO template before deposition. In contrast, alternating current (ac) deposition techniques into PAO templates require fewer processing steps and are more amenable to scale-up but currently provide far less control over the structure of the material deposited. Herein, we report a systematic evaluation of multiple variables that impact ac electrodeposition of Cu into PAO through the resistive, rectifying barrier layer.

The anodization of aluminum has been well documented in the literature and has been used as an industrial process for protecting, strengthening, and coloring aluminum for several decades.[4−6] It has been found that the nature of the resultant oxide is dependent upon applied potential, temperature, and electrolyte. The most commonly used electrolytes for the formation of PAO are sulfuric acid, oxalic acid, and phosphoric acid, depending on the pore diameter and pore density required. Formation of uniform, cylindrical, hexagonally ordered pores requires the use of the two-step anodization process[9−11] or presurface patterning[12,13] and specific anodization conditions for each of the three acids. This specificity stems from the fact that electric fields concentrated at pore tips can explain propagation of pores formed at surficial defects but are insufficient to cause self-ordering of the pores. Self-ordering requires the generation of a suitable mechanical strain at the interface between the Al substrate and the growing Al_2O_3 film. This is achieved when an appropriate volume expansion ratio (approximately 1.4) is achieved through use of suitable anodization conditions (temperature, electrolyte concentration, and voltage).[14] The anodization voltage also controls the interpore spacing and the equilibrium barrier layer thickness, both of which are proportional to voltage employed. The diameter of the pores is specifically related to the electrolyte but may be further tuned by postgrowth etching. A schematic of a porous aluminum oxide template is shown in Figure 1.

Direct current electrodeposition into PAO templates is most commonly performed by removing the remaining aluminum substrate, opening the pore bottoms via etching in phosphoric acid, and finally depositing a conducting layer, such as gold, on one face of the template.[1−3,7,8,15] More recently, Gösele and co-workers have reported a method where the barrier layer was thinned to a thickness proportional to 1 V final anodization potential, at which point the barrier layer is thin enough to enable dc electrodeposition without the prior removal of the aluminum substrate.[16] Using this method, electrodeposition of 30-μm-long silver nanowires was obtained; however, the barrier layer thinning process is time-consuming and must be precisely controlled to ensure that the resultant barrier layer is thinned uniformly.[16] Also recently, Stacey and co-workers have reported dc electrodeposition into PAO formed by depositing silver onto one side of a thin (<100-μm thick) Al foil, preparing an

* Author to whom correspondence should be addressed. E-mail: joel.haber@ualberta.ca.

10.1021/jp051320d CCC: $30.25
Published on Web 08/27/2005

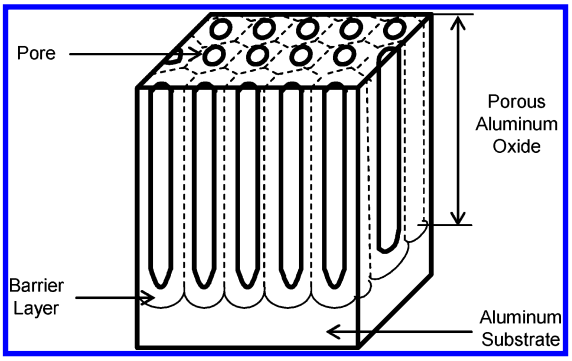

Figure 1. Schematic diagram of porous aluminum oxide template.

electrode, and anodizing the Al completely to the silver film.[17] However, this requires adhesion of a very thin foil to a substrate (such as glass), and it is difficult to uniformly anodize the entire foil completely to the silver film. For industrial scale processes, or applications where a rapid and simple method of template production is required, it is still preferable to develop an ac deposition process which produces wires of comparable length without the involved and sensitive barrier layer thinning process.

Without separation from the barrier layer, or implementation of complex processing strategies such as those outlined above, electrodeposition into PAO templates is only possible under ac conditions, as a result of the aluminum oxide barrier layer at the base of the pores that is formed during the anodization process. This barrier layer blocks direct current with a high resistance of 10^{10} to 10^{12} Ωcm.[18] However, under alternating current, the anodic aluminum oxide conducts preferentially in the cathodic direction and, as such, aluminum is known as a "valve metal."[19] This inherent rectifying property of the barrier layer allows the reduction of ions in the pores during cathodic half-cycles, without allowing reoxidation during the anodic half-cycles.[18−22] However, since the barrier layer is highly resistive, ease of electrodeposition is enhanced by reducing the barrier layer thickness by chemical etching (which also increases the pore diameters) or by electrochemical barrier layer thinning, both of which are simple processes that generally require ∼30−60 min at the end of the anodization.[19,20,23−25] The commonly employed electrochemical thinning is achieved by gradually reducing the anodization voltage to produce a thinner barrier layer, after the pores are grown to the desired depth. A secondary consequence of the reduced voltage is that conditions are no longer appropriate for achieving pore ordering in the electrolyte, and dendritic branching of the pore bottoms is typically observed.[20] For PAO templates formed at higher anodization potentials (and consequently having a thicker barrier layer), some degree of barrier layer thinning is essential to enable electrochemical deposition even under ac conditions.

In general, ac electrodeposition through the barrier layer is a complicated process, as evidenced by the reported variation in the quality of pore-filling (the percentage of pores with material deposited and the variation in the amount of material deposited in each pore) as a function of deposition conditions, including electrolyte concentration, composition, and temperature,[22] and upon deposition voltage, frequency, waveform (sine, square, and triangle),[22,23,26] pulse polarity, and sequence. Moreover, the optimal deposition conditions appear to depend on the metal or compound deposited.[22] This observed complexity is not surprising, because the chemical and structural nature of the barrier layer is complex and ill-defined, particularly after barrier layer thinning. It is also reasonable to expect that the structure of the barrier layer will be modified over the minutes to hours required for the electrodeposition. Add to this the dynamic changes occurring in the barrier layer and the electrolyte in the pores during a single deposition cycle, and optimizing the template preparation and electrochemical deposition conditions becomes a formidable task.

The feasibility of the electrodeposition of copper into the pores of a PAO template under ac conditions from an aqueous metal salt solution has been reported by Moskovits and co-workers. However, experimental details were not reported, and the resultant wires filled on average half the depth of the 5-μm-deep pores.[27] Electrodeposition of other metals (including iron, nickel cobalt, cadmium, bismuth, gold, and silver) into PAO templates under ac conditions has also been reported.[19−22,26,28,29] Nearly all of the reported ac depositions through the barrier layer have been into <25-nm diameter, sulfuric acid grown pores. It is known that the structure and chemistry of the barrier layer grown in oxalic acid differs significantly from that of PAO grown in sulfuric acid;[4] this difference can be expected to impact the ac electrodeposition into the template. In most cases, the quality of pore-filling, in terms of length uniformity of the resultant wires and the height to which the pores were filled, is not reported. In cases in which complete pore-filling has been reported, pore depth has ranged from 600 nm[21] to 2 μm.[28] With pore depths of well over 100 μm available, it is clear that ac techniques capable of uniformly filling much deeper pores would be of use for a variety of applications.

To identify a set of optimized conditions for ac electrodeposition of copper into PAO templates, a systematic study of the effect of multiple variables has been carried out. Promising initial deposition conditions were identified using a fractional factorial design of experiment (FFDOE).[30] FFDOE is a statistical experimental method that enables the simultaneous study of the effect of multiple variables on a response of interest. In this approach, multiple variables are simultaneously changed in each carefully designed experiment rather than changing only one variable while holding all others constant between experiments. The advantages of an FFDOE include determining the effect of several variables using fewer experiments and insight into multiple variable interactions. This experiment examined the effect of final anodization potential (barrier layer thickness), ac deposition voltage, ac deposition frequency, pulsed or continuous deposition, and electrolyte concentration on the quality of pore-filling in oxalic acid grown templates. This resulted in the identification of ac and pulsed ac conditions enabling the filling of 4-μm-deep oxalic acid anodized pores. It also identified damage occurring to the template under continuous deposition conditions, leading to the preferential use of pulsed ac electrodeposition conditions. By rational examination of these results and consideration of the effect of wave shape and pulse polarity, a further optimized set of pulsed ac conditions incorporating a square wave was developed enabling the filling of deeper oxalic and sulfuric acid anodized pores. Quality of pore-filling was determined using scanning electron microscopy (SEM) of pore cross sections and of as-deposited and ion-milled surfaces. The structure and crystallinity of the resultant wires was studied using X-ray diffraction (XRD) of in-situ wires and transmission electron microscopy (TEM) of liberated nanowires.

Experimental Section

Electrode Preparation. All electrodes were constructed from Aldrich or Alfa Aesar high-purity aluminum foil (99.99+%), 1-mm thick, annealed in air at 500 °C for 24 h in a tube furnace. Al pieces, 1.7 cm × 1.0 cm in size, were etched in 1.3 M sodium

TABLE 1: Summary of Deposition Variables Employed for FFDOE

variable level	deposition voltage (V_{rms})	deposition frequency (Hz)	trigger frequency (Hz)	electrolyte (M)	deposition time[a] (min)
low	12	50	20 (pulsed)	0.5 $CuSO_4$/0.57 H_3BO_3	15−25 (pulsed)
high	14	200	200 (continuous)	1.0 $CuSO_4$/0.57 H_3BO_3	1.5−2.5 (continuous)

[a] Deposition time was scaled with deposition voltage over the ranges stated.

hydroxide at 60 °C for 2 min to remove the native oxide layer and to clean and degrease the foil. After etching, the foil was rinsed in distilled water. Two methods of electrode construction were employed. For the FFDOE, an 18-gauge tin-plated copper wire was soldered to the back of the foil with Pb/Sn solder and the back and edges of the electrode and the wire were encapsulated in Dexter Hysol Epoxi-Patch structural adhesive, and the exposed wire was sealed into a 20-cm-long Pyrex tube. For wave shape and pulse polarity experiments, the Al foil was anodized directly on both sides by attaching a copper clip to a portion of the foil not immersed in the electrolyte. A bead of structural adhesive was applied to separate the immersed electrode area from the electrical contact area to provide a well-defined anodization surface and to prevent runaway anodization at the electrolyte/air/aluminum interface. The encapsulation was eliminated on these electrodes to simplify electrode mounting for postdeposition ion-milling.

Immediately prior to anodization, the sodium hydroxide etching was repeated, and each electrode was electropolished at 3 ± 2 °C in a magnetically stirred 100-mL aliquot of a solution composed of 130 mL 70% perchloric acid, 600 mL ethanol, 90 mL 2-butoxyethanol, and 135 mL distilled water.[31] The aluminum electrode was set as the anode against a platinum gauze counter electrode and was electropolished to a mirrorlike finish at 500 mA/cm^2 using a KEPCO BOP 100-1M or Lambda EMS 300-3.5 power supply in three 10-s intervals with 15-s cooling periods between each interval. Following electropolishing, each electrode was rinsed in distilled water.

Anodization of the aluminum electrode was carried out in a two-step process following the methods of Masuda: 0.30 M sulfuric acid at 25.0 V[9] and 0.30 M oxalic acid at 40.0 V.[10] Anodizations were carried out at 3 ± 2 °C with magnetic stirring against a platinum gauze counter electrode. The potential was applied using one of a variety of commercially available or in-house fabricated dc power supplies. Following an initial anodization of 2 h, electrodes were rinsed in distilled water and the oxide layer was etched off in a 1:1 mixture of 0.2 M chromic acid and 0.6 M phosphoric acid at 60 °C for 30 min.[32] This was followed by a second anodization of 2−10 h depending on the electrolyte and the pore depth desired. Growth rates of the PAO layer were approximately 6.0 μm/h in sulfuric acid and 2.4 μm/h in oxalic acid. Pore diameters were 20 and 35 nm in sulfuric and oxalic acid anodized templates, respectively. Following the second anodization, the voltage was systematically reduced to promote thinning of the barrier layer. In oxalic acid, the voltage was lowered by 2 V/min until 30 V was reached, after which the voltage was lowered by 1 V/min until a final anodization voltage of 15 or 10 V was reached, depending on the barrier layer thickness required. The anodization was then continued for 10 min at this final voltage to allow for equilibration of the barrier layer. In sulfuric acid anodized pores, barrier layer thinning was achieved by reducing the voltage by 2 V/min to 19 V, 1 V/min to 10 V, and finally holding the voltage at 10 V for 8 min.

Electrodeposition. Prior to electrodeposition, the edges of the face of the encapsulated electrodes were resealed with epoxy to prevent current leakage through aluminum exposed along the edges of the Al_2O_3 where the Al/Al_2O_3 had been removed from the epoxy during the electropolishing and removal of the Al_2O_3 produced during the first anodization step. On the nonencapsulated electrodes, the back and edges of the electrodes were sealed with nail polish to produce an electrode with only one face exposed. In all cases, the macroscopic active area of the electrodes was approximately 1 cm^2. Each electrode was then immersed in an ultrasonic bath in distilled H_2O for 5−15 min (depending upon pore depth) and was soaked in water for an additional 5 min to ensure thorough pore wetting and then was equilibrated in the deposition bath a further 5 min prior to deposition. For electrodeposition, the ac signal, applied across the PAO electrode and a platinum gauze counter electrode, was generated using a Tabor 8023 arbitrary function generator and was amplified with a KEPCO BOP 100-1M amplifier to the desired voltage.

For the FFDOE, specific conditions for each run were determined by the experimental design (see Supporting Information),[30] with the experimental design and analysis performed using Minitab statistical software (©1972−2004 Minitab Inc., www.minitab.com). Variables were each set at a low and high level, chosen to lie within the condition space expected to produce good quality results on the basis of extensive previous experiments employing a wide variety of sine wave voltages, frequencies, pulse frequencies, barrier layer thinning processes, and electrolyte compositions. All runs were performed on oxalic acid anodized templates with a pore depth of 4 μm and final anodization voltages of 10 or 15 V. The electrodeposition variables employed in the FFDOE are summarized in Table 1.

Wave shape and pulse polarity experiments were carried out using oxalic and sulfuric acid anodized pores, with pore depths of 12.4 ± 0.6 μm (sine wave depositions only) and 24.3 ± 1.2 μm deep pores (sine wave and square wave depositions). In all cases, the final anodization voltage was 10 V. The electrolyte was 0.50 M $CuSO_4$/0.57 M H_3BO_3 for all depositions, and the electrodeposition variables employed for wave shape and pulse polarity experiments were 200 Hz (5-ms duration) waveforms, single pulses triggered at 20 Hz (50-ms intervals), with a sine wave voltage of 13 V_{rms} (18.4 V_{peak}), and a square wave voltage of 17 V_{peak}. Current data was recorded using a Tektronix TDS 1002 digital capture oscilloscope equipped with a compact flash memory module reading a current sense (pin 10) on the KEPCO amplifier. A current trace corresponding to one 5-ms pulse cycle was recorded at the start, middle, and end of each deposition. Deposition times for sulfuric acid anodized pores were 17 min (current trace recorded at 5 and 15 min) and 35 min (current trace recorded at 5, 15, and 30 min) for 12-μm and 24-μm pore depths, respectively. Deposition times for oxalic acid anodized pores were 35 min (current trace recorded at 5 and 30 min) and 75 min (current trace recorded at 5, 35, and 65 min) for 12-μm and 24-μm pore depths, respectively. Using these data, average net charge density (summed over entire pulse width), average component charge density (summed separately for oxidative and reductive components of the pulse), and average current density traces were determined for each set of deposition conditions and pore type.

Square waves used for wave shape and pulse polarity experiments were selected on the basis of preliminary experiments performed using square waves with voltages ranging from 13 to 22 V_{peak}. Pulse frequency and pulse width were also varied with 200 Hz square waves pulsed at 5 Hz, 100 Hz square waves pulsed at 10 Hz, and 80 Hz square waves with 60% duty on the reductive pulse (7.5-ms reductive pulse/5-ms oxidative pulse) triggered at 6.5 Hz. In these preliminary experiments, other variables, such as electrolyte composition and final anodization voltage, remained fixed at those levels which had been identified as optimum for sine wave depositions in the results of the FFDOE. It was found that higher square wave voltages produced inconsistent results, while variations in pulse trigger frequency and pulse width did not noticeably alter the quality of deposition. Qualitatively, the best results were achieved with square wave conditions chosen for pulse polarity and wave shape experiments outlined above. Sine wave conditions for pulse polarity and wave shape experiments were those identified as optimum in the results of the FFDOE.

Characterization of Pore-Filling. The quality of pore-filling (percentage of pores filled and the height to which they were filled) was evaluated by SEM of cross sections and of as-deposited and ion-milled surfaces. Cross sections were prepared by cutting the electrodes from the back until approximately 90% of the aluminum substrate was severed. This was judged by observing the cross section of the electrode visually as well as by the appearance of cracks in the porous alumina surface. The electrode was then pulled apart in the plane of the electrode with force applied perpendicular to the cut. This resulted in a clean exposure of the pore cross sections suitable for characterization of pore-filling and sample depth.

To quantitatively assess the effects of pulse polarity and wave shape on the degree of pore-filling, the as-deposited samples were milled to uniformly expose the pore openings at the surface of the template or at some specified depth below the initial surface. Milling of samples was carried out using an Oxford Ion Fab 300+ ion mill. These surfaces were characterized by SEM, and the percentage pore-filling was determined using Image J image analysis software (Wayne Rasband, Research Services Branch, National Institute of Mental Health, Bethesda, Maryland, http://rsb.info.nih.gov/ij/). All samples were analyzed at three randomly selected points distributed across the surface of the sample, and a representative percentage pore-filling was calculated.

Wire Characterization. Wires were characterized in situ by XRD using a Bruker AXS D8 diffractometer with area detector. Powder patterns were collected on as-deposited samples as well as on samples which had been ion milled to remove surface deposition. Characterization of liberated wires by TEM was performed on a JEOL 2010 TEM equipped with a CCD camera and energy-dispersive X-ray spectroscopy (EDS) system. To prepare TEM samples, wires were liberated in 0.6 M phosphoric acid at 60 °C or in 0.1 M sodium hydroxide at 40 °C. The liberated wires were then rinsed multiple times in distilled water and were finally dispersed in methanol. At each stage, wires were sonicated in an ultrasonic bath for 1−2 min, and solvent exchange was carried out by centrifuging, extracting the supernatant, and adding fresh solvent. To prepare the TEM sample, one drop of the final suspension in methanol was placed on a nickel/lacy carbon TEM grid and the methanol was allowed to evaporate.

Results

Fractional Factorial Design of Experiment. The FFDOE was employed to examine the effect of five variables (final anodization voltage, deposition voltage, deposition frequency, pulsed or continuous deposition, and cupric sulfate concentration) with each variable set at a high and low level, on three different responses: pore-filling as measured by the percentage of pores that were filled completely, wire length dispersity qualitatively categorized on the basis of the difference between the maximum and minimum pore-filling, and pitting of the electrode qualitatively categorized on the basis of the degree of damage to the template. For details on the method and results, see the Supporting Information. A summary of the key results follows.

Pore-Filling. The frequency of the deposition signal had the most significant effect on pore-filling, with the high setting for deposition frequency (200 Hz) producing better results. Pulsed or continuous deposition also impacted the results, with continuous wave depositions resulting in improved pore-filling. While the magnitude of the effect was less, pore-filling was also increased with deposition voltage set at the high level (14 V_{rms}). At the same time, the results indicated that final anodization voltage (and consequently the barrier layer thickness) should be set at the low level (10 V) to maximize pore-filling.

Wire Length Dispersity. In general, results for minimization of dispersity were in agreement with those for maximized pore-filling. The deposition frequency should be set at the high level, continuous deposition should be employed, and cupric sulfate concentration (which was not a statistically significant variable for yield) should be set at its low value (0.5 M).

Template Pitting. The results for minimization of pitting were, in general, opposite to results obtained for maximized pore-filling and minimized dispersion. For the minimization of pitting, the final anodization voltage (and consequently barrier layer thickness) should be set at the high level (15 V), while deposition frequency should be set at the low level (50 Hz) and pulsed deposition employed.

On the basis of the results for pore-filling and wire length dispersity, the following set of optimized conditions was identified: 10 V final anodization voltage, 13 V_{rms} deposition voltage, 200 Hz deposition frequency, continuous wave deposition, and 0.5 M cupric sulfate. An intermediate voltage of 13 V_{rms} was chosen rather than the high level of 14 V_{rms} since the effect of deposition voltage in terms of yield was small, and higher deposition voltage was also linked with increased pitting. These conditions resulted in complete filling of 4-μm-deep oxalic acid anodized pores with monodisperse wires but extreme pitting of the electrode also resulted. SEM micrographs are presented in Figure 2a and b.

In an effort to minimize the pitting of the electrode, the optimized conditions were modified according to the results of the FFDOE when fit with template pitting while still trying to maintain conditions expected to maximize yield and minimize wire length dispersity. To achieve this, all conditions were maintained at the previously stated levels maximizing pore-filling and minimizing dispersity, with the exception of pulse trigger frequency, which was reduced to its minimum value by employing a pulsed wave deposition with a 200 Hz sine wave triggered at 20 Hz. While this resulted in a slight increase in wire length dispersity, good uniformity of pore-filling was maintained and the pitting of the electrode was eliminated. SEM micrographs are displayed in Figure 2c and d. It was found that pitting could also be prevented by ensuring bulk growth did not occur (Figure 2e and f). When continuous wave depositions were employed in sulfuric acid anodized pores, pitting was found to occur to a lesser degree (Figure 2g and h).

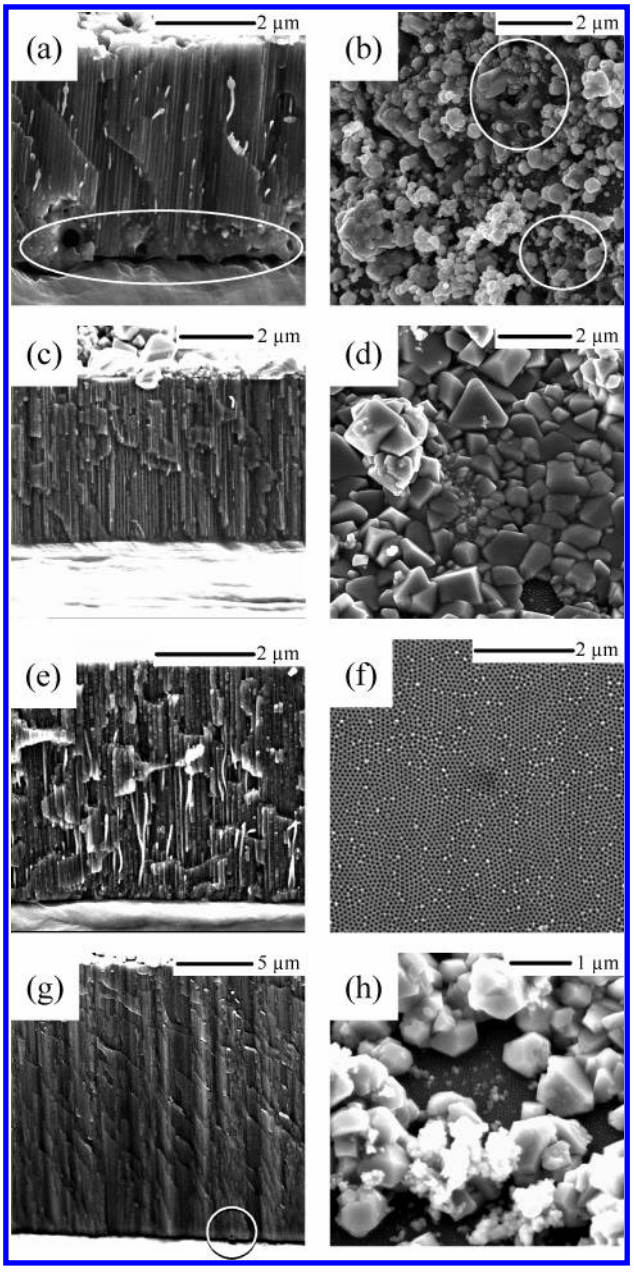

Figure 2. SEM images of oxalic acid anodized templates filled using continuous sine wave deposition with bulk growth (a) and (b), pulsed sine wave deposition with bulk growth (c) and (d), and continuous sine wave deposition without bulk growth (e) and (f). SEM images of sulfuric acid anodized templates filled using continuous sine wave deposition with bulk growth (g) and (h). In samples a−f, pores are 4-μm deep, and in g and h, pores are 25-μm deep. Circles in a, b, and g identify areas of template damage.

Also, in almost all depositions, some overgrowth of the template occurred. This overgrowth results in less wire length dispersity being observed than would be noted if the deposition was immediately halted when wires first reached the surface of the template.

Effects of Pulse Polarity and Wave Shape. On the basis of the three fitting parameters employed in the FFDOE (pore-filling, wire length dispersity, and pitting), the best set of conditions identified incorporated the pulsed sine wave. In ac electrodeposition, the deposition wave shape may be varied, and in pulsed ac electrodeposition the pulse may also be applied in two different polarities; oxidative/reductive or reductive/oxidative. To examine the effect of wave shape and pulse polarity, multiple experiments were executed using pulsed 13 V_{rms} (18.4

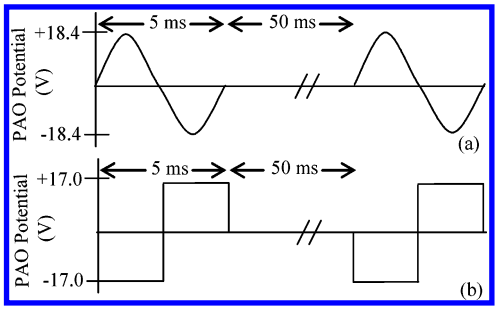

Figure 3. Schematics of two of the wave shapes and pulse polarities employed in this work, pulsed sine wave with oxidative/reductive pulse polarity (a) and pulsed square wave with reductive/oxidative pulse polarity (b).

V_{peak}) sine waves or 17 V_{peak} square waves (200 Hz frequency pulsed at 20 Hz), utilizing each of the possible pulse polarities. Schematics of two of the four possible combinations are illustrated in Figure 3. SEM images of 24-μm-deep sulfuric and oxalic acid anodized templates deposited using sine waves with the different pulse polarities and then milled to expose the surface of samples and a depth of 5 μm below the surface are shown in Figure 4. Figure 5 shows images collected at the surface, and depths of 5, 10, and 15 μm below the surface, of 24-μm-deep sulfuric and oxalic acid anodized templates deposited using square waves with the different pulse polarities. A graphical summary of the percentage pore-filling versus depth below initial sample surface for all four deposition conditions and both sulfuric and oxalic acid anodized templates is presented in Figure 6. In nearly all cases, the percentage of pore-filling increases nearly linearly with depth. A complete set of charge density data, and current traces collected at the midpoint of each deposition, is available in the Supporting Information.

These results identify the impact of both wave shape and pulse polarity on the quality of pore-filling. In all cases, superior pore-filling (measured by the number of pores filled to the surface of the template) was obtained when square wave pulsed electrodepositions were employed. Pulse polarity also impacted the quality of pore filling; however, the polarity that produced the best filling was dependent on the wave shape employed. For sine wave pulsed depositions into pores grown in sulfuric acid (both 12- and 24-μm deep), pulse polarity had no significant effect on the percentage of pores filled to the top of the film (Table 2). In contrast, pulse polarity had a major impact upon the quality of pore-filling for sine wave depositions into pores grown in oxalic acid. In particular, the percentage of 12-μm-deep pores completely filled increased 2-fold when the oxidative/reductive polarity was used rather than the reductive/oxidative pulse polarity. In the 24-μm-deep oxalic acid grown templates, the improvement was significant but not as dramatic. The overall greater pore-filling of 12-μm-deep pores relative to the 24-μm-deep pores is attributed to the decrease in pore depth.

When square wave depositions were employed, the relationship between pulse polarity and filling was reversed, with reductive/oxidative pulse polarity resulting in improved pore-filling (Table 2). Square wave depositions into 24-μm-deep sulfuric acid anodized pores produced pore-filling of 52% and 31% using reductive/oxidative and oxidative/reductive pulse polarity, respectively. The use of reductive/oxidative pulse polarity also resulted in improved deposition with square wave pulsed depositions into 24-μm-deep oxalic acid anodized pores; however, the effect was less pronounced. On the basis of these results, the two best sets of conditions are 13 V_{rms}, 200 Hz sine wave pulsed at 20 Hz with oxidative/reductive pulse polarity,

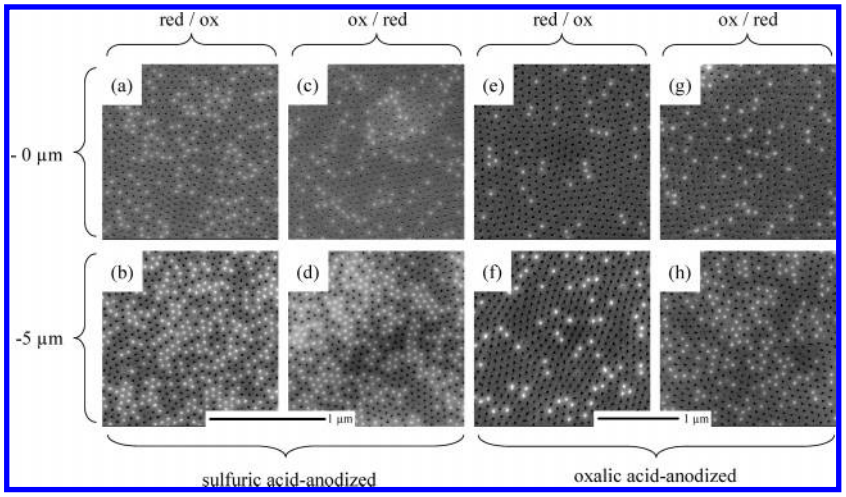

Figure 4. SEM images of 24-μm-deep sulfuric acid anodized (a−d) and oxalic acid anodized (e−h) pores with copper deposited using sine waves with red/ox and ox/red pulse polarity. Samples have been ion-milled to expose the surface, and 5 μm below the original surface, showing the progression of pore-filling as a function of depth. Images a, b and e, f taken progressively from samples deposited using reductive/oxidative pulse polarity. Images c, d and g, h taken progressively from samples deposited using oxidative/reductive pulse polarity.

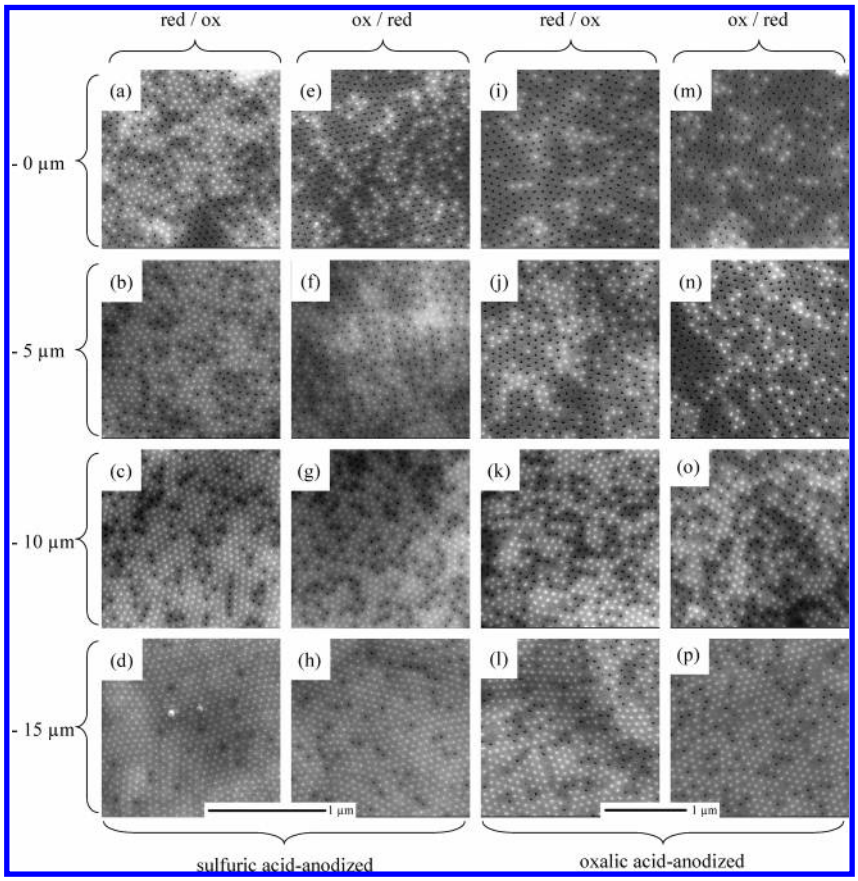

Figure 5. SEM images of 24-μm-deep sulfuric acid anodized (a−h) and oxalic acid anodized (i−p) pores with copper deposited using square waves with red/ox and ox/red pulse polarity. Samples have been ion-milled to expose the surface, and 5, 10, and 15 μm below the original surface, showing the progression of pore-filling as a function of depth. Images a−d and i−l taken progressively from samples deposited using reductive/oxidative pulse polarity. Images e−h and m−p taken progressively from samples deposited using oxidative/reductive pulse polarity.

and 17 V_{peak}, 200 Hz square wave pulsed at 20 Hz with reductive/oxidative pulse polarity, with the square wave pulsed electrodeposition conditions resulting in superior pore-filling. The best pore-filling overall was achieved in sulfuric acid anodized pores using the pulsed square wave with reductive/oxidative pulse polarity resulting in complete filling of greater than 50% of 24-μm-deep pores.

Variations in pore-filling were also found to correlate with variations in current density trace and charge density data, collected during the course of the depositions. Figure 7 shows current density traces corresponding to single 5-ms active pulses collected at the midpoint of sine wave pulsed electrodepositions into 24-μm-deep oxalic acid anodized templates using both reductive/oxidative and oxidative/reductive pulse polarity. Also shown in Figure 7 is component charge density per pulse obtained via separate integration of the reductive component and oxidative component of each current trace. Examination of the current traces indicates that the peak reductive current density during oxidative/reductive pulse polarity depositions is

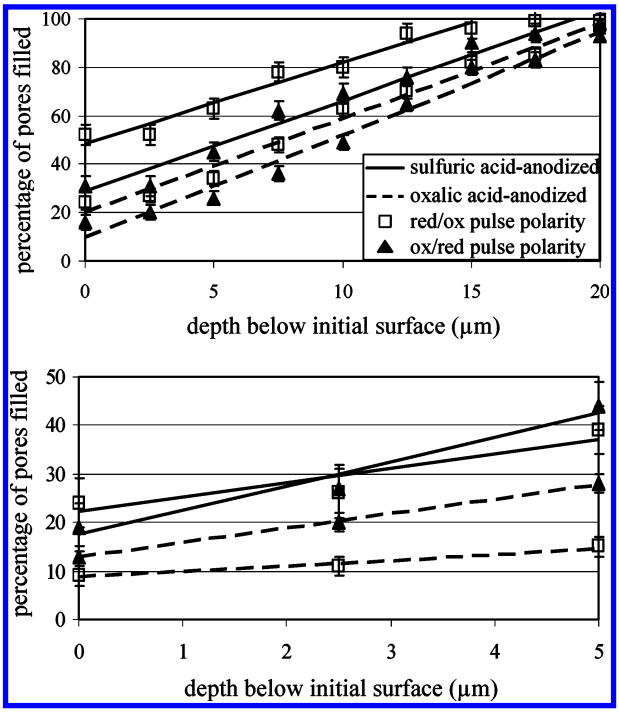

Figure 6. Percentage pore-filling as a function of depth below original surface of the template for 24-μm-deep pores. 17 V_{peak} square wave pulsed depositions (upper plot) and 13 V_{rms} sine wave pulsed depositions (lower plot).

TABLE 2: Summary of Percentage of Pores Completely Filled Using Pulsed Electrodeposition

waveform	pore depth	anodization electrolyte	pulse polarity	percentage filled
sine (13 V_{rms})	12 μm	H_2SO_4	reductive/oxidative	30 ± 3
			oxidative/reductive	32 ± 2
		$(COOH)_2$	reductive/oxidative	10 ± 2
			oxidative/reductive	20 ± 4
	24 μm	H_2SO_4	reductive/oxidative	24 ± 5
			oxidative/reductive	19 ± 2
		$(COOH)_2$	reductive/oxidative	9 ± 2
			oxidative/reductive	13 ± 1
square (17 V_{peak})	24 μm	H_2SO_4	reductive/oxidative	52 ± 4
			oxidative/reductive	31 ± 3
		$(COOH)_2$	reductive/oxidative	24 ± 6
			oxidative/reductive	16 ± 2

approximately 44% (40 mA/cm^2) greater than during reductive/oxidative pulse polarity depositions. When the oxidative and reductive components of the traces were integrated to yield the corresponding component charge density, it was found that the reductive charge per pulse when oxidative/reductive pulse polarity is employed is approximately 50% (20 C/cm^2) greater than when using reductive/oxidative pulse polarity, while the oxidative charge per pulse is approximately equal in both cases (Figure 7). This suggests that increased pore-filling observed with oxidative/reductive pulse polarity sine wave depositions into oxalic acid anodized pores results from increased reductive charge, corresponding to increased reduction of copper. When cross-sectional images are examined, it is clear that wires have grown to a greater height, but there is no indication that significant improvement in the uniformity of deposition and pore-filling accompanies the increased deposition.

When the comparable current density and charge density data is examined for pulsed sine wave depositions into 24-μm-deep sulfuric acid anodized templates (Figure 8), a slight increase in peak reductive current (~4%) and net reductive charge (~10%) is observed with oxidative/reductive pulse polarity relative to

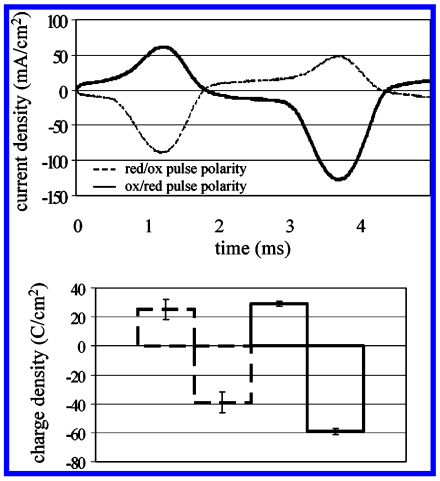

Figure 7. Current density traces (top figure) and component charge density per pulse obtained from integration of current traces (bottom figure), collected during sine wave pulsed electrodepositions into 24-μm-deep oxalic acid anodized pores. Data collected at deposition midpoint (35 min) using reductive/oxidative pulse polarity and oxidative/reductive pulse polarity.

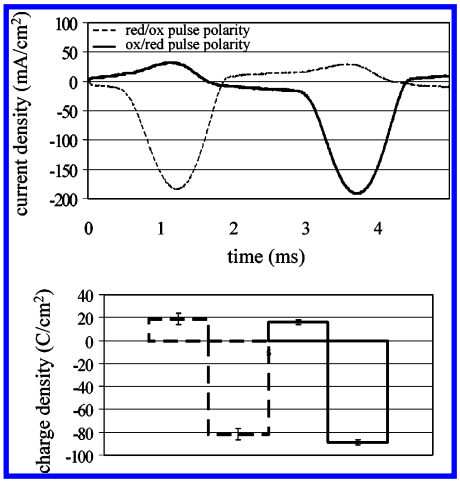

Figure 8. Current density traces (top figure) and component charge density per pulse obtained from integration of current traces (bottom figure) collected during sine wave pulsed electrodepositions into 24-μm-deep sulfuric acid anodized pores. Data collected at deposition midpoint (15 min) using reductive/oxidative pulse polarity and oxidative/reductive pulse polarity.

reductive/oxidative pulse polarity. However, because of the small magnitude of the difference, no change in the magnitude or quality of the deposition is observed.

Conversely, when the current trace density and charge density data for square wave depositions are examined, the most significant variation as a consequence of pulse polarity occurs in the oxidative component of the active pulse. This is illustrated in Figure 9, showing current density traces collected at the midpoint and end point of a square wave reductive/oxidative pulse polarity deposition into 24-μm-deep sulfuric acid anodized pores. While the reductive current density of each pulse is almost identical, the oxidative current density increases significantly over the course of the deposition, with a 5-fold increase in current density at the tail of the current traces. In the corresponding oxidative charge density, an approximately 200% increase (71 C/cm^2) between the midpoint and end point of the deposition is observed (see Supporting Information). With reductive/oxidative pulse polarity and square wave depositions into 24-μm-deep oxalic acid anodized pores, a much smaller increase in the oxidative current density (approximately 2-fold

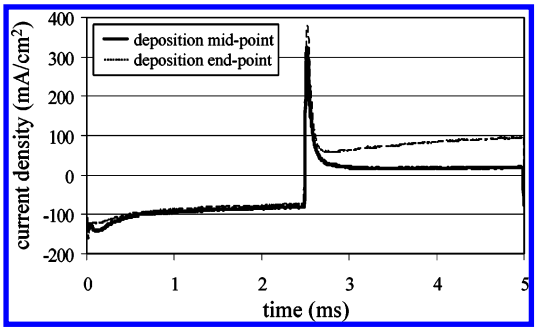

Figure 9. Current density traces collected during square wave pulsed electrodepositions into 24-μm-deep sulfuric acid anodized pores collected at deposition midpoint (15 min) and deposition end point (30 min) shown as solid trace and dotted trace, respectively.

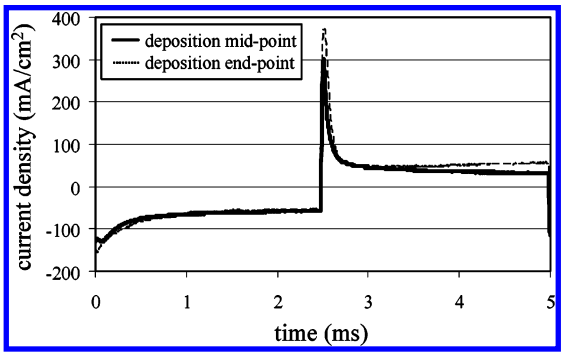

Figure 10. Current density traces collected during square wave pulsed electrodepositions into 24-μm-deep oxalic acid anodized pores collected at deposition midpoint (35 min) and deposition end point (65 min) shown as solid trace and dashed trace, respectively.

at the tail of the current trace) is observed over the course of the deposition (Figure 10). A corresponding increase in oxidative charge density of approximately 31% (18 C/cm^2) between the midpoint and end point of the deposition is also observed (see Supporting Information). When oxidative/reductive pulse polarity is employed, this degree of variation in the oxidative current density over the course of the deposition is no longer observed, and the magnitude of change in oxidative charge density is significantly reduced. In sulfuric acid anodized templates, a lesser increase in oxidative charge density per pulse is observed ($\sim$160%, 30 C/cm^2), while in oxalic acid anodized pores the oxidative charge density per pulse remains constant over the course of the deposition (see Supporting Information).

The summary observation is that while pulsed square wave depositions result in improved pore-filling regardless of pulse polarity relative to pulsed sine wave depositions, the degree of pore-filling increases significantly when reductive/oxidative pulse polarity is employed, with the magnitude of the improvement in pore-filling correlating with the magnitude of the increase in oxidative current density/charge density over the course of the deposition. In pulsed sine wave depositions, variations in pore-filling correlate with variations in the observed reductive current trace density/charge density, with oxidative/reductive pulse polarity leading to increased copper deposition.

Wire Characterization. Wires deposited using the best pulse sequences were shown to be crystalline copper by TEM (Figure 11) and XRD (Figure 12). TEM results suggest that the wires are either single crystalline or composed of several large crystallites that span the diameter of the wire and are on the order of micrometers in length along the wire axis. TEM results also suggest that the as-deposited wires contain numerous crystal defects. EDS results obtained during TEM analysis of liberated wires show the presence of aluminum, likely because of residual

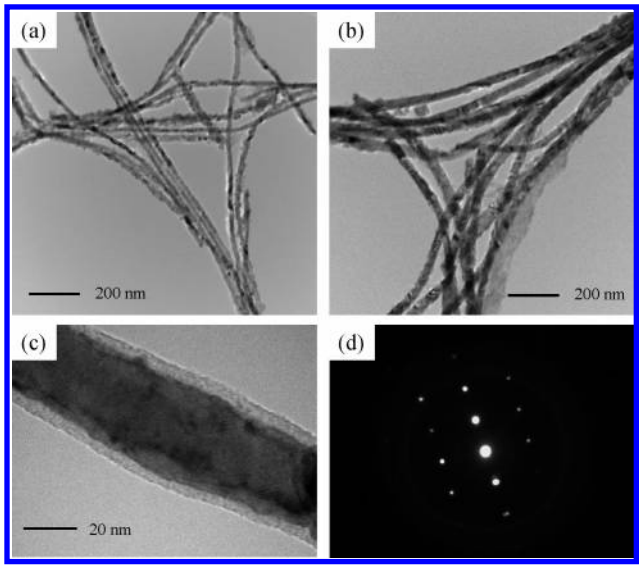

Figure 11. TEM images of (a) wires liberated from sulfuric acid anodized pores (b) and (c) wires liberated from oxalic acid anodized pores and (d) SAED pattern from c.

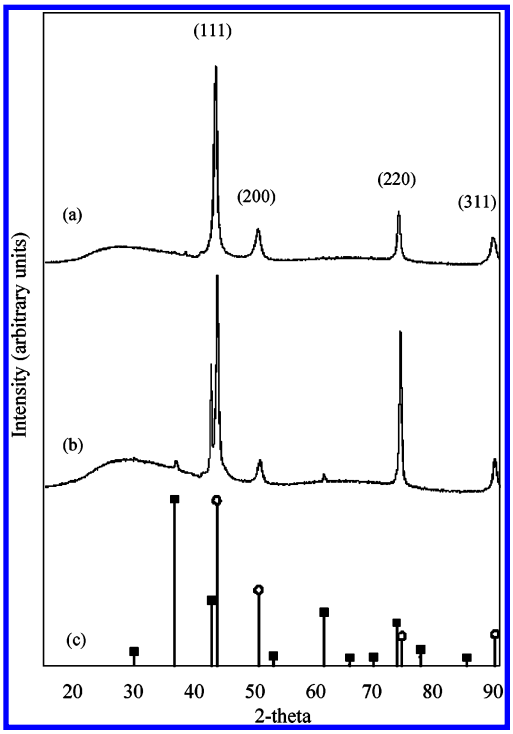

Figure 12. In-situ XRD powder patterns from (a) wires deposited in sulfuric acid anodized pores with ion-milled surface and copper peaks indexed, (b) wires deposited in oxalic acid anodized pores with ion-milled surface, and (c) standard powder patterns for Cu (round heads) and Cu_2O (square heads).

Al_2O_3 not removed during the liberation process. The oxide sheath visible in Figure 11c may also be partially composed of copper oxide resulting from oxidation during or after liberation.

XRD patterns of the as-deposited, unmilled films after 3 days of air exposure (Figure 13) show large copper oxide peaks with a preferred orientation along the [200] direction, with peak positions well matched with those of Cu_2O. These patterns may be compared to those collected following ion-milling to remove bulk growth (Figure 12). The post-ion-milling powder pattern of wires deposited in sulfuric acid anodized pores (Figure 12a, collected 6 days after ion-milling, stored in air) contains no significant copper oxide peaks, and the copper peaks show only

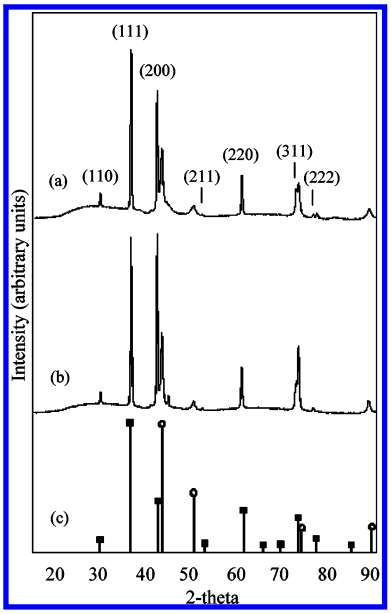

Figure 13. In-situ XRD powder patterns from (a) wires as-deposited in sulfuric acid anodized pores with Cu_2O peaks indexed and (b) wires as-deposited in oxalic acid anodized pores and (c) standard powder patterns for Cu (round heads) and Cu_2O (square heads).

a slight preferred orientation along the [220] direction. In contrast, the post-ion-milling powder pattern of wires deposited in oxalic acid anodized pores (Figure 12b, collected 2 days after milling, stored in air) indicates a much stronger preferred orientation of the copper nanowires along the [220] direction, and Cu_2O peaks are still present with strong preferred orientation along the [200] direction. Furthermore, the copper (220) peaks in both patterns and copper oxide (200) peak in the pattern collected from wires deposited in oxalic acid anodized templates are highly textured, as indicated by nonuniform Debye rings observed during data collection with the area detector. These data suggest that the PAO matrix protects the bulk of the nanowires from oxidation, so that oxidation is confined to the exposed wire tips. We ascribe the absence of copper oxide in the milled sulfuric acid anodized samples to the nearly complete filling of all of the pores; therefore, after ion-milling, the oxidized tips are removed. In contrast, the pores of the oxalic acid grown PAO are not as uniformly filled, such that after ion-milling the oxidized tips of the shorter nanowires remain, with the preferred orientation and texture of the copper oxide related to the preferred orientation of the parent copper nanowires.

Discussion

The difference in pore-filling achieved in sulfuric and oxalic acid is explained by the different chemistry, structure, and properties of the barrier layers resulting from the growth and barrier layer thinning process in these two acids. We explain the superior pore-filling of the oxidative/reductive pulse polarity over that of the reductive/oxidative pulse polarity upon application of pulsed sine waveforms as resulting from polarization effects in the electrolyte during the rest period between pulses. Most importantly, we argue that square waveforms produce better pore-filling with the opposite reductive/oxidative polarity because migration of cationic defects in the Al_2O_3 barrier during the deposition pulses increases resonant tunneling through the barrier layer. The effect of this increased tunneling over the course of the deposition is a reduction in rectification of the barrier layer, increased oxidative current flow, and reduced net

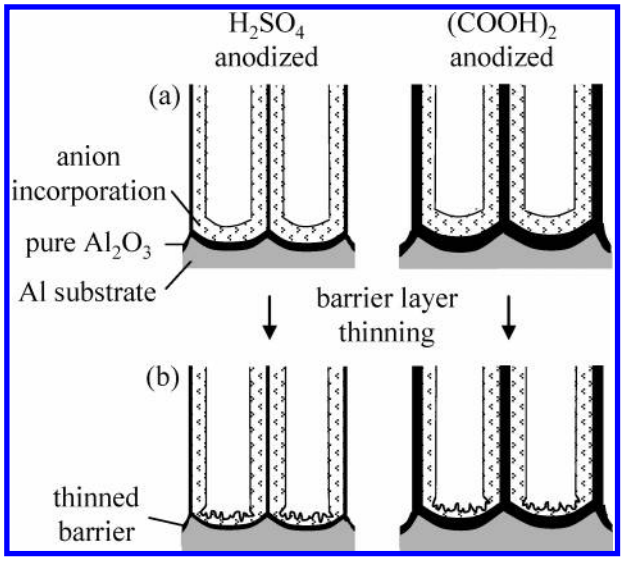

Figure 14. Schematic of PAO pore bottoms showing (a) compositional variation as a function of anodizing electrolyte and (b) structural change that results from thinning of the barrier layer to facilitate ac electrodeposition.

copper deposition into the pores with the thinnest barrier layers, enabling the pores with initially more resistive barrier layers to "catch-up".

Structure of Pore Bottoms and Barrier Layer in PAO. The structure of porous aluminum oxide has been, and continues to be, the subject of intensive investigation.[4−6,33,34] Although the schematic honeycomb structure of porous alumina presented in Figure 1 is widely used and accurately reflects the physical structure of as-grown, well-ordered porous alumina, it does not accurately reflect the chemical complexity of the as-grown porous alumina. A more accurate representation of the physical and chemical structure of as-grown PAO is shown in Figure 14a. Porous aluminum oxide is, in fact, not pure Al_2O_3 but incorporates significant amounts of the acid anion into the walls and barrier layer.[4] Moreover, these acid anions are not uniformly distributed throughout the barrier layer or pore walls but are concentrated on the electrolyte side of the layer, while the middle of the walls and Al side of the barrier layer is essentially pure Al_2O_3. Furthermore, the total amount of acid anion incorporation, and fraction of the barrier layer incorporating the acid anion, depends primarily upon the acid type and secondarily upon the anodization conditions (voltage, temperature, and possibly concentration).[4,33,34] The chemical, mechanical, and electrical properties of the anion incorporating layers are quite different from those of pure Al_2O_3. Typical concentrations of acid anion incorporation are 12−14 wt % sulfate and 2−4 wt % oxalate. Correlated with these amounts of anion incorporation, the relative thickness of the pure Al_2O_3 portion of the barrier layer is less for pores grown in sulfuric acid (∼5%) than in oxalic acid (∼10%).[4,33,34] Because the pure Al_2O_3 layer is proportionately thinner in sulfuric acid grown pores than in oxalic acid grown pores, the anodization current and growth rate is much greater in sulfuric acid than in oxalic acid. It is also known that the acid ion incorporating layer has a much higher rate of chemical etching than the relatively pure alumina layer.

The gradual reduction of the voltage to reduce the barrier layer not only reduces the thickness of the barrier layer but alters the pore size and distribution at the pore bottoms. This produces a thin, branched (possibly dendritic) structure at the bottom of the uniform pores rather than the test tube bottoms that are produced if the anodization is simply stopped.[20] A schematic

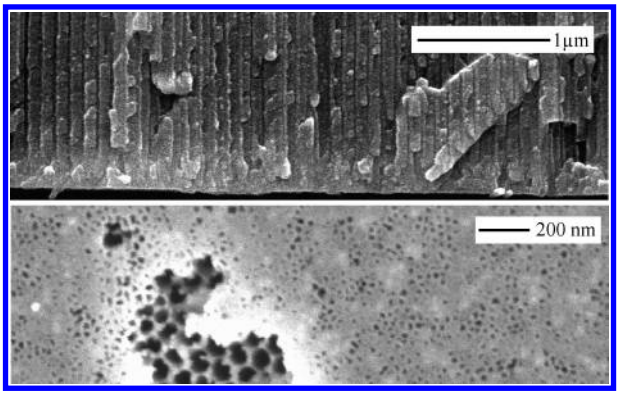

Figure 15. SEM images showing disordered layer that forms during barrier layer thinning. Top image shows cross section with ordered pores transition to disordered barrier layer. Lower image shows bottom view with aluminum substrate removed and pores partially opened via dissolution in phosphoric acid. Large openings are ordered pores, and small openings are smaller disordered pores formed at reduced voltage during the barrier thinning process.

representation of the barrier thinned pores is shown in Figure 14b. SEM images collected from pore cross sections and bottoms which have been subjected to our electrochemical thinning process are presented in Figure 15, showing the physical structure that is depicted schematically in Figure 14b. To our knowledge, the impact of the thinning process on the structure of the pores in this thin, nonuniform layer and upon the relative thickness of the pure and impure sections of the barrier layer has not been investigated. Clearly, the exact nature of these structures will depend on the rate of voltage decrease. At a sufficiently slow rate, the steady-state structure (and interpore spacing) will be maintained throughout the process, producing a branched pore structure with the expected barrier layer thickness and relative thicknesses of the pure and impure layers. At a sufficiently rapid rate of voltage decrease, the rate of electrochemical barrier layer thinning will not keep up with the rate of voltage decrease, and the current will fall to zero. At this point, the much slower chemical etching will predominate over the electric field assisted anodization process, and the impure portion of the barrier layer will be preferentially removed, leaving a proportionately larger fraction of the pure Al_2O_3 portion of the barrier layer. In practice, we have selected a barrier layer thinning process that was as rapid as possible to minimize both the pore branching and the thickness of the dendritic layer relative to the ordered layer while still retaining a measurable anodization current. Because similar barrier layer thinning protocols were used both in sulfuric and oxalic acid and because the rate of anodization is much slower in oxalic acid, we expect that the structure of the barrier layer will deviate from the steady-state ratio in oxalic acid more than in sulfuric acid. That is, we expect the fraction of the pure alumina portion of the barrier layer to be enhanced in the oxalic acid anodized material more than in the sulfuric acid anodized material. This difference in composition is thought to contribute to the different results for sulfuric and oxalic acid grown pores for the different electrodeposition processes.

Uniform Electrodeposition into PAO. To fill all pores uniformly and completely, it is necessary to achieve a consistent growth rate in all pores. As individual wires reach the surface of the electrode ahead of the growth front in other pores, they will inhibit the growth of wires in unfilled pores in two ways. First, wires in contact with the bulk electrolyte provide an electrical pathway of lowered resistance. In those pores, where wires have yet to reach the surface of the template, mass transfer limitations within the pore result in increased resistance relative

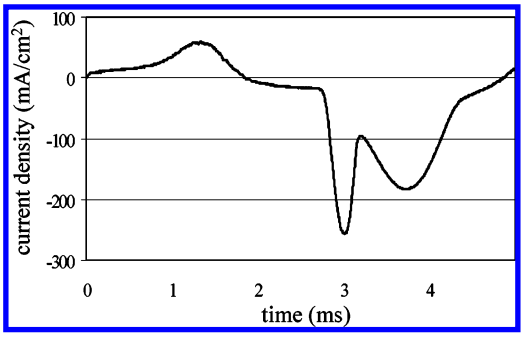

Figure 16. Current density trace collected at the end of a deposition in sulfuric acid anodized pores showing the presence of a lower potential shoulder peak resulting from bulk deposition

to the bulk electrolyte. As a result, reductive current will be preferentially shunted through the wire or wires in contact with the bulk electrolyte, limiting the growth of the wires in the partially filled pores. This is experimentally supported by the observation of shoulder peaks on current density traces at a lower potential position on the sine wave that develop as the deposition proceeds, and bulk growth becomes evident. An example of this shoulder peak is shown in Figure 16 for deposition into sulfuric acid anodized pores. Second, bulk growth on the surface of the electrode with pulsed depositions is in the form of crystalline polyhedra, which block access to the 10−100s of pores surrounding them, limiting further growth in those pores. As a result, it is critical to obtain consistent growth rates of all wires to achieve complete pore filling.

One approach to controlling the growth rate of the wires is to maintain a uniform and controlled potential at the wire growth front. If this potential is maintained at the minimum potential required for the reduction of metal ions, slow and uniform wire growth would occur in all pores. This approach is commonly used for controlled dc metal deposition into PAO templates.[35] In ac deposition through the barrier layer, this is not feasible for two reasons. First, the barrier layer exhibits small, random fluctuations in thickness[28] that will correspond to random fluctuations in resistance. Second, since the barrier layer thinning process results in disordered growth of branched or dendritic pores that decrease in spacing and diameter, the structure of the porous layer at the bases of the pores will be variable (Figures 14b and 15). This will produce variations in the area of the pore bottoms and consequently the current density in the pore, further complicating the matter.

A second general approach to producing uniform growth is via control of reactant availability. In this case, reactant availability is controlled by diffusion of metal ions from the bulk electrolyte to the wire growth front. Continuous ac depositions maintain a state of ion depletion in the pores at all times; consequently, the growth rate is limited by diffusion of ions along the length of the pore. Since constant bulk electrolyte concentration is maintained at the electrode surface via stirring and since the pore diameters are produced with a narrow size distribution, the rate of diffusion and the subsequent wire growth rate are expected to be consistent among the pores resulting in uniform wire growth and complete pore-filling. In pulsed ac deposition, maintaining diffusion-controlled growth is more challenging.

Gösele and co-workers have reported that increased uniformity of growth may be achieved via application of relatively high constant current density pulses.[28] A high current density results in high nucleation rates, which is followed by wire growth. In pores that have a thinner barrier layer, metal ions are rapidly depleted, resulting in increased resistance in the pore

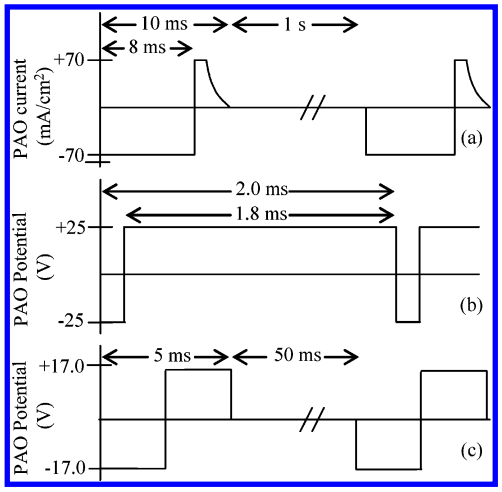

Figure 17. Deposition sequences used by Gösele and co-workers (a), Metzger and co-workers (b), and in the current work (c).

electrolyte. This will result in increased current flow in pores with a thicker barrier layer and higher metal ion concentration allowing them to catch-up. Between pulses, a rest period is used during which no current is applied to allow reequilibration of the electrolyte concentration in the pores.[28] A schematic of the deposition sequence used by Gösele and co-workers is presented in Figure 17a. However, if a current control method is to be implemented consistently, it is critical to have well-defined electrode areas. As previously mentioned, the dendritic pore structure produced during the barrier layer thinning process is irregular and ill-defined; therefore, reproducibly producing large-area electrodes with identical active deposition areas may be precluded. For a simple and convenient method of deposition, it is preferable to use voltage-controlled waveforms that are insensitive to electrode area. Metzger and co-workers have reported that uniform growth of wires in 600-nm-deep pores was achieved using a continuous square wave, where a short reductive pulse was followed by an extended oxidative pulse.[21] A schematic of the voltage-controlled deposition sequence used by Metzger and co-workers is presented in Figure 17b and may be contrasted with the best voltage-controlled sequence used in the present work in Figure 17c.

Continuous versus Pulsed Electrodeposition. Diffusion-limited growth was achieved using continuous wave depositions, which as a result yielded superior pore-filling in the results of the FFDOE. Qualitative evidence that diffusion-limited growth was occurring under the continuous wave regime is the observation that less active deposition time was required to yield a comparable amount of metal deposition using pulsed electrodeposition than using continuous electrodeposition. Unfortunately, continuous wave conditions were also accompanied by template damage. Metzger and co-workers have also reported observing template damage when employing the deposition sequence illustrated in Figure 17b and have speculated that it is due to aluminum oxide hydroxide dissolution producing hydrogen gas.[21] We believe that the observed damage in our work results from ohmic heating, an explanation that is consistent with the fact that damage is only observed when deposition proceeds to bulk growth, an event that is accompanied by increased current density corresponding to rapid deposition of metal from the bulk electrolyte and, consequently, increased ohmic heating. Other possible implications of continuous wave depositions include reduced crystallite dimensions of the as-deposited wires. Schmid and co-workers have performed detailed X-ray characterization of copper nanowires deposited using continuous wave ac conditions similar to those used in this work and have reported an average crystallite size of 12 nm.[36] In contrast, the copper nanowires we have produced using pulsed electrodeposition are nearly single crystalline. This distinction is also made evident by the observation that overgrowth from continuous wave ac conditions are spherical and of nanometer dimensions while overgrowth from pulsed deposition conditions consists predominantly of large, faceted crystallites (Figure 2b and d).

The FFDOE results showed that electrode damage could be eliminated by using pulsed wave deposition conditions with only a modest decrease in quality of pore-filling in 4-μm-deep oxalic acid anodized pores. The elimination of template damage and the ability to grow predominantly single-crystalline wires make the use of pulsed electrodeposition appealing. It is also expected that pulsed deposition conditions should be less affected by increasing pore depths than by continuous deposition conditions, where diffusion limitation and ion depletion are expected to impact wire growth. The challenge with pulsed electrodeposition is that uniform growth in all pores is more difficult to achieve since metal ion concentration at the growth front is no longer diffusion-rate-limited. Ion depletion occurs during the reductive pulse, with the concentration at the wire tip then returning to bulk concentration during the period of zero applied potential. In pores which are significantly deeper than those used in the FFDOE, the impact of this is expected to be magnified, with wire length dispersion increasing with pore depth.

Effect of Waveform. A rationalization for our improved results obtained with square wave depositions relative to that achieved with sine wave depositions follows intuitively from the discussion of slower growing pores being able to catch-up during the duration of the pulse. In a sine wave deposition, peak potential is realized for only a small fraction of the 2.5-ms pulse width, and the effective pulse width where the potential is above the minimum required for current flow is relatively short. In a square wave deposition, the step nature of the potential change makes the effective and actual pulse widths identical at 2.5 ms. The fact that we observed substantially improved deposition and pore-filling when implementing the square wave lends support to the catch-up theory proposed by Gösele and co-workers.[28]

Effect of Pulse Polarity. In addition to wave shape, we also examined the effect of pulse polarity, something that has not yet been reported in the literature. On the basis of the concept that the oxidative component of the pulse removes the capacitive charge buildup across the barrier layer that occurs during the reductive component, all pulsed depositions reported to date have employed reductive/oxidative pulse polarity. In this work, increased deposition over an identical time period was observed when the oxidative/reductive pulse polarity was employed rather than the reductive/oxidative pulse polarity, in conjunction with sine wave depositions. However, when square wave depositions were employed, the conventional reductive/oxidative pulse polarity produced the most uniform pore-filling.

These two phenomena are a consequence of different processes occurring during the course of the deposition; however, we argue that both are a direct consequence of the structure and composition of the aluminum oxide barrier layer and the dynamic changes that occur therein during the course of the deposition. Once metal deposition into the pores has begun, the metal/insulator/electrolyte structure is replaced by the metal/insulator/metal structure. In contrast to dc electrodeposition, which may be regarded as standard electrodeposition through a nanostructured deposition mask, ac deposition inherently requires electron transport through this device. The quality

of the metal deposition will critically depend on how the MIM capacitor responds to the deposition sequence, a response that we have found varies with deposition conditions. These results indicate that the PAO should not be regarded as a simple template for ac electrodeposition but rather should be treated as a dynamic variable affecting the outcome of the deposition process.

Sine Wave Pulses. The effect of pulse polarity on pore-filling for the sine wave pulses is explained by the nature of the electrical double layer resulting from charge stored on the barrier layer during the zero potential periods between active pulses. When oxidative/reductive pulse polarity is employed, negative charge will be stored on the barrier layer, and the resultant electrical double layer will incorporate copper cations to balance charging at the wire tip. It is well-known that adsorption of species at an electrode surface can impact the kinetics of electron transfer,[37] and it is thought that adsorption or increased concentration of copper ions resulting from the formation of the electrical double layer results in the observed increase in deposition rates. This relies on the adsorption or increased concentration persisting during the oxidative pulse, which is thought to be the case. A rough estimate of the diffusion distance of copper cations during the oxidative pulse is obtained by calculating the root−mean−square displacement on the basis of the diffusion coefficient and elapsed time ($D = 7.14 \times 10^{-6}$ cm^2/s, $t = 2.5$ ms) where $\Delta = \sqrt{(2Dt)}$.[37] This yields a diffusion distance of less than 2 μm and does not take into account any specific adsorption, ensuring that the increased concentration or adsorption will largely persist during the oxidative pulse. Since the effective width of the sine wave reductive pulse is very short (<2.5 ms), a significant fraction of the ions reduced during the pulse are those that had been incorporated into the electrical double layer. Consequently, increased electron transfer or deposition rates are observed when using oxidative/reductive pulse polarity relative to reductive/oxidative pulse polarity with sine wave pulsed electrodeposition.

The difference in the magnitude of the effect between oxalic and sulfuric acid anodized templates is a consequence of difference in the structure and composition of the barrier layer. In sulfuric acid anodized pores, the barrier layer is inherently thinner because barrier layer thickness is proportional to anodization voltage, and the large difference in initial barrier layer thickness between sulfuric and oxalic acid anodized pores is maintained to some degree during the thinning process. As previously discussed, the composition and thickness of the barrier layer is also modified during the thinning process, with the relative thickness of pure alumina remaining relatively constant in sulfuric acid anodized pores, while the relative thickness of the pure alumina layer in oxalic acid anodized pores increases. This is borne out experimentally by the significantly larger current densities and shorter deposition times observed during electrodeposition into sulfuric acid anodized pores relative to oxalic acid anodized pores. As a consequence of this variation in barrier layer thickness and composition, less charge is stored on the barrier layer during the zero potential periods between active pulses during depositions into sulfuric acid anodized templates, and fewer metal cations are incorporated into the electrical double layer or are adsorbed at the tip of the growing wire.

The magnitude of the difference in capacitive charging may be approximately quantified by comparing the average oxidative charge density per pulse, which is 25 C/cm^2 for oxalic acid anodized templates compared to 20 C/cm^2 for sulfuric acid anodized templates. This difference may be attributed directly to the charge stored on the barrier layer, and if it is recognized that these figures are convoluted with any oxidative current that is passed, it is likely that the difference in stored charge is underestimated since leakage current density varies as an inverse exponential with thickness of the insulating oxide layer.

Square Wave Pulses. When square wave pulsed electrodepositions are employed, effects of the electrical double layer are still observed as a variation in the magnitude of net reductive charge passed with differing pulse polarities. However, since the effective pulse width is equivalent to the actual pulse width at 2.5 ms, the ions incorporated into the electrical double layer are a smaller fraction of the total number reduced during a single pulse and consequently the effect is not observed in SEM analysis of pore-filling. Nonetheless, pulse polarity does impact the quality of deposition when square waves are employed; however, the quality of pore-filling is observed to correlate with increasing oxidative current over the course of deposition when the reductive/oxidative pulse polarity is used. We speculate that this increase in oxidative current occurs because of resonant tunneling which is enhanced over the course of the deposition by migration of higher oxidation state aluminum defects.

When an aluminum/aluminum oxide/metal junction is formed with a metal that has a work function greater than that of aluminum, it is known that the junction will act to rectify current; specifically, because of the asymmetric nature of the potential barrier, current will be passed preferentially when the aluminum is biased as the cathode. Conductance through and dielectric breakdown of anodic oxides on Al and other valve metals has been extensively studied experimentally and theoretically for several decades. Although complete consensus regarding the processes has not yet been achieved, the presence of ionic impurities has a large impact on the potential barrier in a metal/insulator/metal junction. In 1965, Schmidlin modeled the trapezoidal potential barrier that results when a potential is applied across a dielectric layer between two metals and the impact of ionic impurities on the shape of this barrier and the implications this has for electron tunneling through the MIM junction.[38] His calculations show that a cationic impurity located in the dielectric film near the metal polarized as the cathode has the effect of substantially reducing the barrier height and of producing what is akin to two potential barriers separated by a potential well. It was qualitatively recognized that because of the reduction in barrier height adjacent to the metal cathode, thermally excited carriers could more easily surmount the barrier with the junction polarized in this direction. He further calculated that a single positive ion per unit area equal to the square of the film thickness (corresponding to one cationic impurity per 100 nm^2 for our ∼10-nm-thick barrier layers) can increase the current through the barrier by an order of magnitude.[38] Subsequent researchers have tended to emphasize the increase in tunneling current enabled by cationic defects over the enhancement of thermal emission over the barrier.[39] Mujica and Ratner have also calculated the rate of tunneling through single rectangular potential barrier relative to a barrier with a discrete structure of wells and barriers for metal/molecule/metal (MMM) junctions.[40] Their calculations also show that the inclusion of potential wells in a potential barrier greatly enhances tunneling rates relative to a continuous potential barrier.[40] Ratner and others have also considered the increased current these defects in the molecular layer may enable through a thermally activated hopping mechanism.[41,42] On the basis of these calculations, it is expected that cationic defects in the alumina layer of PAO templates will have a similar impact on tunneling barriers and conductivity through the alumina layer. In particular, if these

defects are located adjacent to the copper-filled pore or are distributed throughout the barrier layer, they can lead to increased electron transport when the electrode is biased in the anodic direction (copper biased as the cathode), reducing or eliminating the inherent rectification of the aluminum/aluminum oxide/metal junction.

It is also known that these aluminum ion defects may become mobilized under direction of a potential applied across the MIM junction. Such an effect has been reported in aluminum/anodic aluminum oxide/silver junctions[39] with aluminum oxide layers that are of comparable thickness to those encountered in our PAO templates. Hassel and Diesing report that as-grown anodic aluminum oxide contains a fixed density of higher oxidation state centers that are stable up to the formation voltage (the voltage applied during growth of the anodic oxide). Upon application of potentials greater than the formation voltage, defect migration occurs, with increasing voltage increasing the rate of migration. Migration rates are also enhanced by increased temperature. Activation of defect migration is not observed on time scales of <1 ms. As defects align themselves across the barrier layer, resonant tunneling rates may approach those observed with direct tunneling through much thinner barriers.[39] We expect that a similar phenomenon is occurring in our pulsed square wave electrodepositions, with defect migration leading to increased rates of resonant tunneling, thereby decreasing the rectifying effect of the barrier layer.

In sulfuric acid anodized templates, ionic defects are less stable because of lower formation voltages and tend to migrate more readily than those defects formed via anodization in oxalic acid. The migration rate is further enhanced when reductive/oxidative pulse polarity is employed, since ohmic heating during the reductive pulse results in greater defect mobility during the oxidative pulse. Furthermore, it is expected that these effects would be most pronounced in those pores with thinner barrier layers. These pores require the migration of fewer defects to achieve high rates of resonant tunneling, and because of higher current density, increased ohmic heating leads to increased rates of defect migration. During deposition, these pores initially fill faster, but defect migration leads to resonant tunneling and increased oxidative current until rectification is ineffective in that pore. As a result, copper metal is reoxidized and the rate of growth slows in these pores. This allows other pores, with thicker barrier layers that continue to rectify current, to catch-up. In oxalic acid anodized pores, the effect is less pronounced since the higher anodization potential increases the stability of ionic impurities formed during anodization, which reduces defect migration during the subsequent electrodeposition.

This gradual onset of oxidative breakdown in sulfuric acid anodized templates when reductive/oxidative pulse polarity is employed with square wave deposition sequences is further supported by the observation of significant gas evolution in the final minutes of the deposition. This was not observed with any other deposition sequences, and when the as-deposited electrodes were examined, it was found that a nearly solid copper electrode had formed on the surface (see Supporting Information). It is expected that the gas evolution observed was the result of water oxidation at the surface of the electrode, a consequence of the barrier layer modification that had occurred in a large number of pores by this stage of the deposition. This gas evolution is not attributed to reduction of water or protons since a similarly solid copper electrode was formed when oxidative/reductive pulse polarity was employed but no gas evolution was observed (see Supporting Information). It is thought that this process does not occur to any appreciable degree with pulsed sine wave depositions since the root−mean−square voltage is too low to significantly activate defects, and the effective pulse width is below the time required for appreciable defect migration to occur.

We argue that ionic defect migration has led to enhanced deposition uniformity of copper into sulfuric acid anodized templates when reductive/oxidative pulse polarity square waves are employed. It is not clear if this result is general for other metals. It has been found that the field-emitting properties of the second metal in the junction is likely to influence the breakdown voltage, with increasing work function of the metal leading to increased breakdown strength.[43] We do expect, however, that our results on pore-filling as a function of deposition conditions, including wave shape and pulse polarity, should be useful for optimizing the electrodeposition of other metals into PAO templates.

Conclusions

Our systematic investigation of the effect of the deposition waveform on the uniformity and completeness of copper deposition through the barrier layer into PAO templates grown in sulfuric or oxalic acid enables us to reach the following conclusions:

1. Continuous deposition produces the best pore-filling but damages the PAO template and copper nanowires when deposition is continued until bulk copper is deposited on the surface of the PAO film. This damage is much more pronounced for the 35-nm diameter pores grown in oxalic acid than in the 20-nm diameter pores grown in sulfuric acid. This damage is likely caused by ohmic heating during bulk electrodeposition.
2. Pulsed electrodeposition conditions will produce good uniformity of deposition into relatively deep pores without damage to the PAO template or nanowires when deposition is continued to bulk deposition onto the surface of the PAO film.
3. Square waveforms yield better pore-filling than comparable sine waveforms.
4. Pulse polarity significantly impacts the rate and uniformity of pore-filling, but the specific effect is dependent upon both the waveform and the structure and chemistry of the barrier layer.
5. Highly uniform deposition into oxalic acid grown pores by ac deposition is significantly more challenging than deposition into sulfuric acid grown pores because of the different chemistry and structures of the barrier layers.
6. Under the influence of some electrodeposition sequences, changes in the rectification of the barrier layer will occur over the course of the deposition. These changes may determine the quality of pore-filling achieved.

Acknowledgment. The authors would like to acknowledge George D. Braybrook for collection of SEM images and the University of Alberta NanoFab for use of ion-milling facilities. Funding was provided by an NSERC discovery grant (#238526) to J.A.H. N.J.G. thanks NSERC and Alberta Ingenuity for graduate studentships.

Supporting Information Available: Method and results for fractional factorial design of experiment and additional supporting figures. This material is available free of charge via the Internet at http://pubs.acs.org.

References and Notes

(1) Martin, C. R. *Science* **1994**, *266*, 1961−1966.
(2) Hulteen, J. C.; Martin, C. R. *J. Mater. Chem.* **1997**, *7*, 1075−1087.
(3) Shingubara, S. *J. Nanopart. Res.* **2003**, *5*, 17−30.

(4) Thompson, G. E.; Wood, G. C. Anodic Films on Aluminum. In *Corrosion: Aqueous Processes and Passive Films*; Scully, J. C., Ed.; Treatise on Materials Science and Technology, Vol 23; Academic Press: New York, 1983; 205−329.

(5) Thompson, G. E. *Thin Solid Films* **1997**, *297*, 192−201.

(6) Diggle, J. W.; Downie, T. C.; Goulding, C. W. *Chem. Rev.* **1968**, *69*, 365−405.

(7) Tian, M. L.; Wang, J. U.; Kurtz, J.; Mallouk, T. E.; Chan, M. H. W. *Nano Lett.* **2003**, *3*, 919−923.

(8) Nicewarner-Pena, S. R.; Freeman, R. G.; Reiss, B. D.; He, L.; Pena, D. J.; Walton, I. D.; Cromer, R.; Keating, C. D.; Natan, M. J. *Science* **2001**, *294*, 137−141.

(9) Masuda, H.; Hasegwa, F.; Ono, S. *J. Electrochem. Soc.* **1997**, *144*, L127−L130.

(10) Masuda, H.; Fukuda, K. *Science* **1995**, *268*, 1466−1468.

(11) Masuda, H.; Yada, K.; Osaka, A. *Jpn. J. Appl. Phys.* **1998**, *37*, L1340−L1342.

(12) Masuda, H.; Yamada, H.; Satoh, M.; Asoh, H.; Nakao, M.; Tamamura, T. *Appl. Phys. Lett.* **1997**, *71*, 2770−2772.

(13) Choi, J.; Luo, Y.; Wehrspohn, R. B.; Hillebrand, R.; Schilling, J.; Gösele, U. *J. Appl. Phys.* **2003**, *94*, 4757−4762.

(14) Li, A. P.; Muller, F.; Birner, A.; Nielsch, K.; Gösele, U. *J. Appl. Phys.* **1998**, *84*, 6023−6026.

(15) Zhang, X. Y.; Zhang, L. D.; Lei, Y.; Zhao, L. X.; Mao, Y. Q. *J. Mater. Chem.* **2001**, *11*, 1732−1734.

(16) Choi, J.; Sauer, G.; Nielsch, K.; Wherspohn, R. B.; Gösele, U. *Chem. Mater.* **2003**, *15*, 776−779.

(17) Sander, M. S.; Prieto, A. L.; Gronsky, R.; Sands, T.; Stacy, A. M. *Adv. Mater.* **2002**, *14*, 665−667.

(18) Sellmyer, D. J.; Zheng, M.; Skomski, R. *J. Phys.: Condens. Matter* **2001**, *13*, R433−R460.

(19) AlMawlawi, D.; Coombs, N.; Moskovits, M. *J. Appl. Phys.* **1991**, *70*, 4421−4425.

(20) Nielsch, K.; Muller, F.; Li, A.-P.; Gösele, U. *Adv. Mater.* **2000**, *12*, 582−586.

(21) Sun, M.; Zangari, G.; Shamsuzzoha, M.; Metzger, R. M. *Appl. Phys. Lett.* **2001**, *78*, 2964−2966.

(22) Yin, A. J.; Li, J.; Jian, W.; Bennett, A. J.; Xu, J. M. *Appl. Phys. Lett.* **2001**, *79*, 1039−1041.

(23) Sun, M.; Zangari, G.; Metzger, R. M. *IEEE Trans. Magn.* **2000**, *36*, 3005−3008.

(24) Routkevitch, D.; Bigioni, T.; Moskovits, M.; Xu, J. M. *J. Phys. Chem.* **1996**, *100*, 14037−14047.

(25) Masuda, H.; Tanaka, H.; Baba, N. *Bull. Chem. Soc. Jpn.* **1993**, *66*, 305−311.

(26) Preston, C.; Moskovits, M. *J. Phys. Chem.* **1993**, *97*, 8495−8503.

(27) Davydov, D. N.; Sattari, P. A.; AlMawlawi, D.; Osika, A.; Haslett, T. L.; Moskovits, M. *J. Appl. Phys.* **1999**, *86*, 3983−3987.

(28) Sauer, G.; Brehm, G.; Schneider, S.; Nielsch, K.; Wherspohn, R. B.; Choi, J.; Hofmeister, H.; Gösele, U. *J. Appl. Phys.* **2002**, *91*, 3243−3247.

(29) AlMawlawi, D.; Liu, C. Z.; Moskovits, M. *J. Mater. Res.* **1994**, *9*, 1014−1018.

(30) Box, G. E. P.; Hunter, W. G.; Hunter, J. S. *Statistics For Experimenters*; John Wiley & Sons: New York, 1978.

(31) Li, F.; Zhang, L.; Metzger, R. M. *Chem. Mater.* **1998**, *10*, 2470−2480.

(32) Li, A. P.; Muller, F.; Birner, A.; Nielsch, K.; Gösele, U. *J. Vac. Sci. Technol., A* **1999**, *17*, 1428−1431.

(33) Vrublevsky, I.; Parkoun, V.; Sokol, V.; Schreckenbach, J.; Marx, G. *Appl. Surf. Sci.* **2004**, *222*, 215−225.

(34) Vrublevsky, I.; Parkoun, V.; Sokol, V.; Schreckenbach, J. *Appl. Surf. Sci.* **2004**, *236*, 270−277.

(35) Gao, T.; Meng, G.; Wang, Y.; Sun, S.; Zhang, L. *J. Phys.: Condens. Matter* **2002**, *14*, 355−363.

(36) Benfield, R. E.; Grandjean, D.; Dore, J. C.; Wu, Z.; Kroll, M.; Sawitowski, T.; Schmid, G. *Eur. Phys. J. D* **2001**, *16*, 399−402.

(37) Bard, A. J.; Faulkner, L. R. *Electrochemical Methods*, 2nd ed.; John Wiley and Sons: New York, 2001.

(38) Schmidlin, F. W. *J. Appl. Phys.* **1966**, *37*, 2823−2832.

(39) Hassel, A. W.; Diesing, D. *Thin Solid Films* **2002**, *414*, 296−303.

(40) Mujica, V.; Ratner, M. A. *Chem. Phys.* **2001**, *264*.

(41) Joachim, C.; Ratner, M. A. *Nanotechnology* **2004**, *15*, 1065−1075.

(42) Joachim, C.; Ratner, M. A. *Proc. Natl. Acad. Sci. U.S.A.* **2005**, *102*, 8801−8808.

(43) Shousha, A. H. M. *J. Non-Cryst. Solids* **1975**, *17*, 100−108.